Soft Matter

COMMUNICATION

View Article Online
View Journal | View Issue

Cite this: *Soft Matter*, 2022, **18**, 8223

Received 7th July 2022,
Accepted 24th October 2022

DOI: 10.1039/d2sm00918h

rsc.li/soft-matter-journal

The elastic response of graphene oxide gels as a crumpling phenomenon

Sebastian Barwich and Matthias E. Möbius *

The broad spectrum of chemical and electronic properties of 2D nanomaterials makes them attractive in a wide range of applications, especially in the context of printed electronics. Therefore, understanding the rheological properties of nanosheet suspensions is crucial for many additive manufacturing techniques. Here, we study the viscoelastic properties of aqueous suspensions of graphene oxide nanosheets. We show that in the gel phase, the magnitude of the elastic response and its scaling with volume fraction is independent of the lateral size of the particles and the interaction strength between them. We explain this behavior by modelling the elasticity of these gels as a crumpling phenomenon where the magnitude of the response is determined by the bending stiffness and thickness of the sheets. Due to their low bending stiffness these nanosheets crumple upon deformation and may therefore be considered soft colloids. Furthermore, we provide an explanation why the yield strain decreases with packing fraction for these gels.

Suspensions of attractive, colloidal particles form a stress-bearing, solid-like microstructure beyond a critical particle volume fraction ϕ_c. The magnitude of the elastic response of these particulate gels is an important characteristic and crucial for many industrial processes. In general, the shear modulus G increases with the particle volume fraction ϕ. The two most common scalings observed are $G \propto \phi^n$ where the prefactor and exponent is usually governed by the interaction potential between the particles and the microstructure of the arrested state,[1–6] and a percolation-type scaling $G \propto (\phi - \phi_c)^n$ which has been seen in suspensions of carbon nanotubes,[7] few layer graphene,[8] clays[9] and graphene oxide.[10] In the case of sheets of nanometric thickness (nanosheets) such as graphene[8] and graphene oxide[10–12] the scaling exponent n is between 2.7 and 3.0, though the origin of this scaling remains unknown. Due to their low bending stiffness and high aspect ratio (lateral size/thickness), nanosheets can easily fold and crumple[13–15] and may therefore be considered soft particles. We address the deformable nature of nanosheets which so far has not been considered in the modelling of the elastic response of gels formed by these particles.

Here we show that the strength of the elastic response of nanosheet gels is dominated by the mechanical properties of the nanosheet rather than the interaction between the particles. We find that the scaling exponent of the elastic response with volume fraction is consistent with a crumpling process. Furthermore the magnitude of the elastic response is independent of the lateral size of the particles and the interactions strength between them which is consistent with a crumpling process in which the elastic response is solely governed by the bending stiffness and thickness of the sheets. We show that this model is also consistent with the elastic response of graphene[8] and LAPONITE® suspensions.[9] Finally, we develop a model that explains the decrease of the yield strain with volume fraction and links it to the cohesive energy between particles. This result provides an important insight into the rheology of nanosheet gels as it connects the macroscopic response of the gel to the mechanical properties of single nanosheets which can be considered soft colloids.

We investigate the rheological properties of aqueous graphene oxide (GO) gels as a function of particle volume fraction ϕ and interaction potential which can be changed *via* the addition of NaCl. Graphene oxide is an oxidised graphene monolayer that is usually chemically exfoliated *via* the Hummers' method.[16] These nanosheets can be produced in a wide range of lateral sizes, ranging from approximately 10 nm to several 100 microns, and can have different level of oxidation depending on the preparation method.[17] GO is easily dispersed in water due to the presence of the oxide groups. We obtained aqueous GO stock solution from Graphenea with a concentration of 25 g l^{-1} and a monolayer content >95%. The GO monolayers have a thickness of $h = 0.8 \pm 0.2$ nm[16] and a lateral size of $L_0 = 15 \pm 5$ μm, which we verified with SEM, giving rise to an aspect ratio $\alpha = L_0/h = 18\,750$. One day prior to the rheological measurements we dilute the stock solution to the desired concentration and keep the pH neutral for enhanced

School of Physics, AMBER and CRANN Research Centres, Trinity College Dublin, Dublin 2, Ireland. E-mail: mobiusm@tcd.ie; Tel: +353-01-896-1055

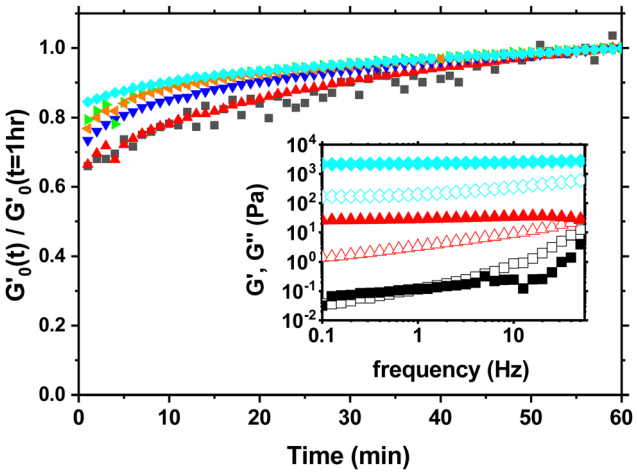

Fig. 1 Time evolution of storage modulus plateau G'_0 normalised by its value 1 hour after loading for different volume fractions ϕ measured at f = 1 Hz and γ_0 = 0.01. (■) 0.00232, (▲) 0.00348, (▼) 0.00463, (▶) 0.00579, (◀) 0.0087, (◆) 0.0116. Inset: G' (solid symbols) and G'' (open symbols) *versus* frequency at ϕ = 0.00232(■,□), ϕ = 0.00348(▲,△) and ϕ = 0.0116(◆,◇).

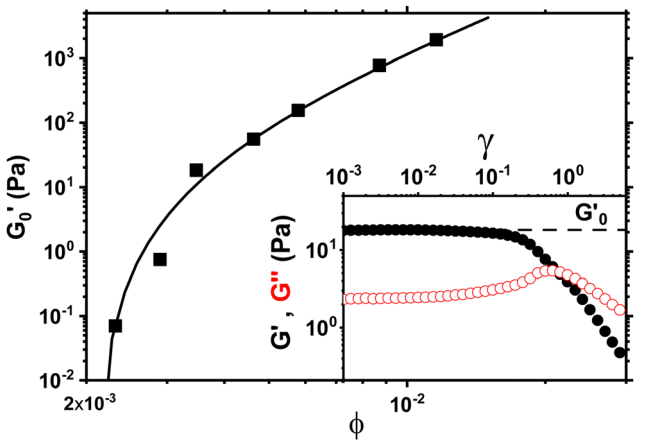

Fig. 2 Storage modulus plateau G'_0 *versus* volume fraction ϕ. Line corresponds to 0.45 GPa $(\phi - \phi_c)^{2.7}$ with ϕ_c = 0.00207. Inset: Strain sweep at f = 1 Hz for ϕ = 0.00348. Dotted horizontal line denotes the storage modulus plateau G'_0.

stability[18,19] by adding appropriate amounts of 0.5 M NaOH. In this work we investigated volume fractions between ϕ = 0.001 and 0.01 that we calculated using 2000 kg m^{-3} as the density of GO. The samples are sonicated for 30 minutes and allowed to rest for 24 hours. After loading the samples into the rheometer we wait for one hour before measurements commence. All rheology measurements are performed in a 5 cm diameter plate–plate geometry at a 0.5 mm gap with roughened plates and a solvent trap to prevent slip and evaporation. We do not preshear the sample as the rheology of GO gels is highly dependent on the flow history.[20,21]

During that 1 hr waiting time we monitor the evolution of the storage modulus G' through small amplitude oscillations in the linear viscoelastic regime to investigate the aging process as shown in Fig. 1. The storage modulus G' is frequency independent and larger than the loss modulus G'' at low frequencies indicating solid like behavior (inset Fig. 1). During the waiting time G' increases between 35% to 20% depending on the concentration with the largest increase occuring in the first 30 minutes. The slight increase in the modulus beyond 60 minutes is negligible for the subsequent measurements and analysis.

In order to measure the elastic response of the GO gel we perform strain sweeps from which we infer the storage modulus G'_0 plateau in the linear viscoelastic regime which corresponds to the shear modulus. The inset in Fig. 2 shows a typical strain sweep where the storage modulus G' is constant and larger than the loss modulus G'' in linear response. Beyond the yield strain, the microstructure disintegrates and the suspensions fluidizes when $G'' > G'$. Fig. 2 shows the shear modulus at different volume fractions which does not follow a simple power law $\propto \phi^n$ but instead is well fit by $G \propto (\phi - \phi_c)^n$, with an exponent $n = 2.7 \pm 0.1$ and ϕ_c = 0.0021. This exponent is consistent with previous rheological experiments on aqueous GO gels[10–12] which are shown Fig. 3A together with our data. Interestingly, not only is the exponent the same, but also the prefactor of this power law despite the fact the lateral size of the GO particles differs by two orders of magnitude between the data sets ranging from 0.6 μm (Valles *et al.*[12]) to 64 μm (Corker *et al.*[11]).

The elastic response of GO gels is similar to other suspensions of nanosheets with a thickness of 1 nm. Both aqueous LAPONITE® clay at different salt concentrations[9] (α = 30) and 3-layer graphene in NMP[8] (α = 1000) do not follow a simple power law either (lower inset Fig. 3B) but are well described by $G \propto (\phi - \phi_c)^n$ with the same exponent (n = 2.7) as GO (Fig. 3B), though the best fit for LAPONITE® is slightly lower (n = 2.35).[9]

While the elastic response of GO gels appears to be independent of lateral size of the particles, the critical concentration ϕ_c at which gelation occurs does depend on it and usually decreases with increasing aspect ratio.[26] In order to quantify the microstructure at ϕ_c, we look at the average free volume V_f per particle, which is defined as $\phi = L_0^2 h/V_f$. Approximating this volume as a simple cube, the size of the free volume $L = V_f^{1/3}$ normalised by the lateral size of the particle gives $L_c/L_0 = 1/(\phi_c \alpha)^{1/3}$ at the gelation point, where $\alpha = L_0/h$ is the aspect ratio of the particles. Two common models to predict ϕ_c are the overlap concentration (OC)[8,27] and the random contact equation (RCE).[26] OC approximates the gelation point as a random packing of imaginary spheres in which the sheets are embedded and can freely rotate in, which leads to $\phi_c = 3\phi_{RCP}/(2\alpha)$. Using the random close pack density of spheres ϕ_{RCP} = 0.64, OC predicts L_c/L_0 = 1.01 at the gelation point ϕ_c. The RCE is based on the orientational average of the excluded volume and predicts for discs that $\phi_c = 2\langle z \rangle/(\pi\alpha)$, where $\langle z \rangle$ is the average contact number per particle. For a random packing of ellipsoids the maximum value is $\langle z \rangle$ = 12,[28] leading to L_c/L_0 = 0.51. The inset of Fig. 3A shows L_c/L_0, the normalized size of the free volume at ϕ_c for the different aspect ratios of the particles shown in the main panels and the predictions made by OC and RCE. Note that for LAPONITE® clays, ϕ_c decreases significantly with salt with a corresponding increase of L_c/L_0 from 1.6 to 3 as the increased particle attraction from the

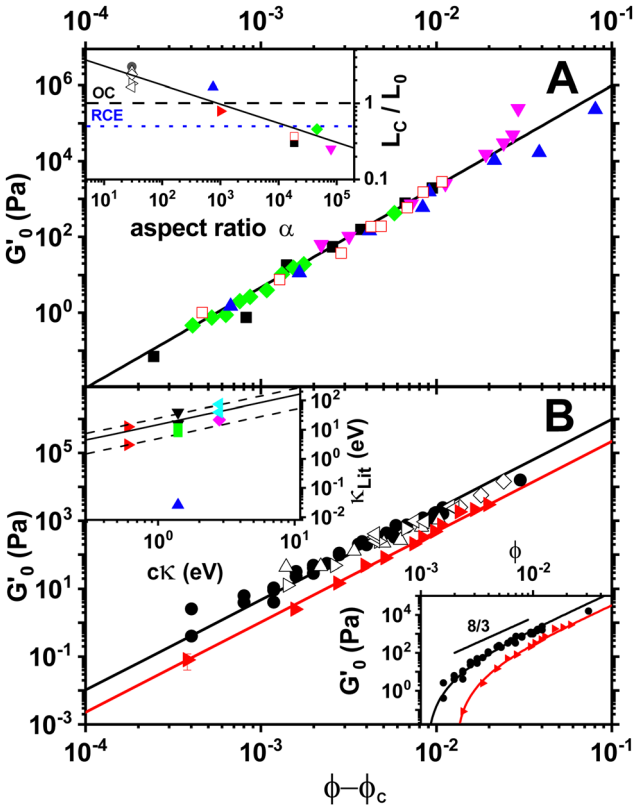

Fig. 3 (A) Storage modulus plateau G'_0 *versus* reduced volume fraction $(\phi - \phi_c)$ for different aqueous GO gels. Black line is eqn (1) with $c\kappa/h^3$ = 0.45 GPa. Our data with L_0 = 15 μm: (■) without NaCl, ϕ_c = 0.00207, (□) 0.1 M NaCl, ϕ_c = 0.0011. Literature data: (▲) Valles *et al.*,[12] L_0 = 0.6 μm, ϕ_c = 0.0003, (◆) Data from supplementary information of Naficy *et al.*,[10] L_0 = 50 μm, ϕ_c = 0.00023, (▼) Corker *et al.*,[11] L_0 = 64 μm, ϕ_c = 0.0008. Inset: Normalised size of the average particle free volume at ϕ_c for the data shown in main panels (A and B) (same symbols as in main panels). Black dashed line corresponds to overlap concentration (OC) L_c/L_0 = 1.01 and blue dotted line to random contact equation (RCE) prediction L_c/L_0 = 0.51, solid black line is a guide to the eye $L_c/L_0 = 5.5\alpha^{-0.25}$. (B) G'_0 *versus* reduced volume fraction $(\phi - \phi_c)$ for different nanosheet gels. Black line is eqn (1) with $c\kappa/h^3$ = 0.45 GPa, red line is eqn (1) with $c\kappa/h^3$ = 0.1 GPa. (▶) 3-layer graphene in NMP,[8] h = 1 nm, L_0 = 1 ± 0.5 μm, ϕ_c = 0.002. Aqueous LAPONITE® clay[9] (h = 1 nm, L_0 = 30 nm) at different NaCl concentrations: (●) 10 mM, ϕ_c = 0.0012, (△) 6 mM, ϕ_c = 0.0017, (◇) 5 mM, ϕ_c = 0.0023, (▷) 3 mM, ϕ_c = 0.0054, (◁) 0.1 mM, ϕ_c = 0.0074. Upper inset: Literature values for the bending stiffness κ_{Lit} *versus* $c\kappa$ from fits to eqn (1). (▶) range of bending angle dependent κ for 3-layer graphene,[22] (▲) GO value from Poulin *et al.*,[23] (■) GO(2 : 1 hydroxyl/epoxide ratio) minimum and maximum value from Liu *et al.*,[24] (▼) GO minimum and maximum value from Incze *et al.*,[25] (◀) range of curvature dependent κ for Montmorillonite (h = 1 nm) from Fu *et al.* (using $\kappa \approx 2r_c^2E_b$, where r_c is the radius of curvature and E_b the bending energy/area), (◆) F-hectorite (h = 1 nm), black and dotted lines denote $\kappa_{Lit} = (15 \pm 10)c\kappa$. Lower inset: G'_0 *versus* ϕ for (▶) 3-layer graphene and (●) 10 mM NaCl LAPONITE® with fits to eqn (1) with the same fit parameters as in main panel.

addition of salt leads to more porous structures.[29–31] L_c/L_0 decreases from 2.3 ± 0.7 (LAPONITE®) to 0.25 for the largest aspect ratio GO particle gel which is just below the RCE prediction for a glassy, random packing of ellipsoids. The value of L_c/L_0 for non-aqueous 3-layer graphene gel is consistent with this overall trend. This shows that the microstructure is not only affected by the particle interactions but also by the aspect ratio.[32] The overall decrease of L_c/L_0 with α ($L_c/L_0 \sim \alpha^{-0.25}$) explains why ϕ_c for all the gels shown only differ by a factor of ≈30 at most across 4 orders of magnitude in aspect ratio as $\phi_c = (L_c/L_0)^{-3}\alpha^{-1} \sim \alpha^{-0.25}$. Since the low aspect ratio GO gel (α = 750) is significantly more porous (L/L_0 = 1.6) compared to the high aspect ratio GO gels ($L/L_0 \approx 0.3$) with $\alpha > 10^4$, the microstructure of GO gels does not appear to play a dominant role in determining the prefactor and exponent of the power law fit to the elastic response in Fig. 3A.

Next, we added NaCl to the suspension in order to increase the interaction between the particles and investigate its effect on the storage modulus plateau of the gel. Adding salt decreases the electrostatic repulsion and makes the potential well between particles deeper up to the critical coagulation concentration (CCC). While the CCC for aqueous GO can be predicted from DLVO theory,[19] DLVO alone may not give a complete description of the interparticle potential.[33,34] Here, the salt concentration was 0.1 M, below the CCC of our gel. The addition of NaCl lowers the critical volume fraction from 0.00207 to 0.0011 analogous to what has been found in LAPONITE® clays[9] (inset Fig. 3A) and consistent with an increased attraction between the particles.[29,30] However, G'_0 still follows the power law with the same exponent and prefactor as shown in Fig. 3A. Therefore the increased interaction leads to changes in microstructure indicated by the change of ϕ_c but does not alter the overall strength and scaling of the elastic response.

Existing models[1–6] for gel elasticity cannot account for this observation as the magnitude of the elastic response in these models scales with the bond stiffness between the particles. These models assume that particles are stiff and the elasticity arises solely from the interaction between the particles and the overall microstructure. However, GO particles cannot be considered stiff.[34]

While GO has a relatively high 2D Young's modulus, $Y_{2D} \approx 300$ N m^{-1},[35] its bending stiffness κ is low though there is a considerable spread of values for κ in the literature. The only experimental value is 0.025 eV,[24] a factor of ∼40 lower than graphene and three orders of magnitude smaller than simulation results (up to 40 eV).[24,25] Therefore, the ratio of stretching to bending energies $Y_{2D}L_0^2/\kappa$, the Föppl–von Kármán number,[13] is at least 10^{10} which means that GO and other nanosheets can easily crumple and wrinkle.[14] The elastic response of the GO gel may therefore originate from the stored elastic energy of wrinkles and ridges in the GO rather than the bond stiffness between the particles.

In general, the elastic energy of a crumpled sheet is stored mostly in the ridges[35,36] and can be approximated as a summation of all the ridge energies in a crumpled sheet $E = N\kappa(X/h)^{1/3}$, where N is the number of facets, κ the bending stiffness, X the characteristic size of the ridge and h the thickness of the sheet. The number of facets is simply the area of the sheet divided by the area of the facet $N \sim L_0^2/X^2$ and the random orientation of the facets implies that $N \sim V/X^3$, where V is the volume which the sheet is confined in. Finally, the volume fraction for a single sheet is given by $\phi_s = L_0^2h/V$. These relations lead to an energy density $\varepsilon = E/V \sim (\kappa/h^3)\phi_s^{8/3}$.[36] The Young's modulus Y scales with the energy density. Treating the

crumpled sheet as an elastic, isotropic medium, the shear modulus G is proportional to the Young's modulus with a prefactor of order 1 that depends on the Poisson ratio. Therefore $G \sim Y \sim \varepsilon$. We now model the gel as a suspension of crumpled nanosheets. In such a system crumpling only occurs beyond the gelation threshold ϕ_c, at which the particles touch and form a stress bearing microstructure. Therefore we replace ϕ_s with $(\phi - \phi_c)$ and the shear modulus of the gel can be written as

$$G = \frac{c\kappa}{h^3}(\phi - \phi_c)^{\frac{8}{3}} \quad (1)$$

where ϕ is the volume fraction of the sheets in the suspension and c an unknown constant. Note that in classical elasticity theory, $\kappa \propto h^3$, however this relation does not apply to layered nanosheets,[22,37] therefore the prefactor κ/h^3 may change with nanosheet thickness. Moreover, the effective bending stiffness κ may vary with the radius of curvature.[22,38]

Eqn (1) provides an excellent fit to the data shown in Fig. 3A and is consistent with the observation that the prefactor and exponent is independent of the lateral size and interaction potential. We find that the prefactor $c\kappa/h^3 = 0.45 \pm 0.5$ GPa, which corresponds to a bending stiffness $\kappa = 1.4 \pm 0.2$ eV for $h = 0.8$ nm assuming $c = 1$, which is similar to graphene and inbetween the literature values.[24,25,33] Fitting eqn (1) to 3-layer graphene and LAPONITE® gels (Fig. 3B) yields 0.63 ± 0.15 eV and 2.8 ± 0.8 eV for $c\kappa$, respectively. The literature value for 3-layer graphene is between 3 and 19 eV depending on the bending angle.[23] There are no literature values for LAPONITE®, but κ for other 1 nm thin clay particles from the smectite family range from 22 eV (f-hectorite[39]) up to to 73 eV (montmorrilonite[40]). It may seem surprising that bending should play a role for low aspect ratio LAPONITE® ($\alpha = 30$). However, clay platelets are very compliant and readily conform to nanoscale features.[15] Kinks with radii of curvature as lows as 3 nm have been observed[40] and the energy to create a fold is independent of the lateral particle size. In the case of GO, MD simulations of small GO flakes interacting in water ($\alpha = 13$) have shown significant bending.[41]

While there is considerable spread in κ for each type of nanosheet,[42] the trend is consistent with the literature values being proportional to $c\kappa$ inferred from eqn (1) as shown in the upper inset of Fig. 3B though the experimental value for GO[24] is an outlier. This allows us to constrain the value of the constant $c = (15 \pm 10)^{-1} = 0.066 \pm 0.044$ in eqn (1) from the fit $\kappa_{Lit} = (15 \pm 10)c\kappa$. This leads to a bending stiffness of 21 ± 14 eV for GO similar to simulation results,[24,25] while for 3-layer graphene and LAPONITE® we obtain 9.5 ± 6.3 eV and 42 ± 28 eV, respectively.

In order to gain further insight into the microstructure of the stress-bearing network we measured yield strain as a function of volume fraction. We define the yield strain γ_y to be the point at which G' has decreased a factor of 10 from its plateau value at low strain amplitudes. At this point the gel has lost most of its elasticity due to the strain induced breakage of the microstructure. We rescale the storage moduli from oscillatory strain sweeps by their plateau value G'_0 and yield strain as shown in Fig. 4. The yield strain is decreasing with increasing

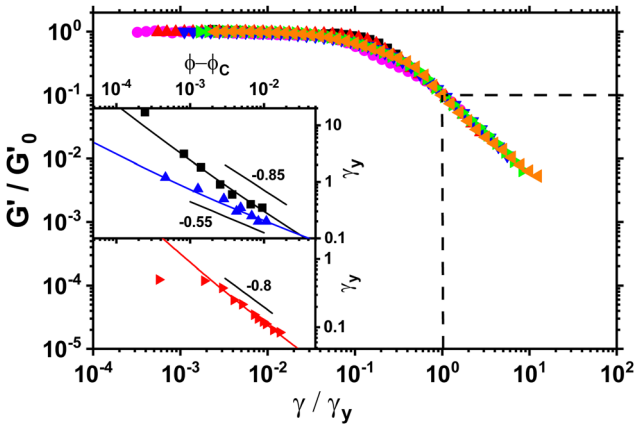

Fig. 4 G' normalised by its plateau value G'_0 *versus* the strain amplitude γ normalised by the yield strain γ_y at $f = 1$ Hz as shown in inset. Data shown from gels without NaCl. $G'(\gamma_y) = 0.1G'_0$ as indicated by the dotted lines. (■) 0.00232, (●) 0.0029, (▲) 0.00348, (▼) 0.00463, (▶) 0.00579, (◀) 0.0087, (◆) 0.0116. Upper inset: The yield strain *versus* $(\phi - \phi_c)$. (■) without NaCl, (▲) with 0.1 M NaCl. The short black lines denote the logarithmic slopes as shown. The lines are fits to eqn (2) with $\sigma = 1.1 \pm 0.2$ mJ m^{-2}, $x = 0.66 \pm 0.05$ without NaCl and $\sigma = 11 \pm 2$ mJ m^{-2} and $x = 1.33 \pm 0.05$ for 0.1 M NaCl using $c\kappa/h^3 = 0.45$ GPa for both fits. Lower inset: The yield strain *versus* $(\phi - \phi_c)$ for 3-layer graphene in NMP gel[8] (▶). The line is a fit to eqn (2) with $\sigma = 7 \pm 0.2$ μJ m^{-2}, $x = 0.7 \pm 0.05$ using $c\kappa/h^3 = 0.1$ GPa.

volume fraction for gels with and without NaCl. Note that a similar trend has been observed in graphene gels[8] and also for carbon nanotube suspensions.[7]

This decrease in γ_y is also seen in gels with fractal microstructures, where theory[32,39] predicts that $G'_0 = f(k_0/L_0)\phi^{(1+\beta)/(3-d_f)}$ and $\gamma_y \propto \phi^{(1-\beta)/(3-d_f)}$ assuming stiff particles. Here, β and d_f are related to the fractal dimensions of the elastic backbone and the flocs, respectively, k_0 is the bond rigidity and f a prefactor. Far from ϕ_c we find that the exponent of the yield strain is -0.55 (-0.85) for the GO gels with (and without) salt. Using $G'_0 \sim \phi^{2.7}$ this results in $\beta = 1.5(1.9)$ and $d_f = 2.1(1.9)$ which is similar to what has been found in other gels.[22] However, the addition of salt should increase the bond rigidity k_0 and thereby G'_0, which is not what we observe. Also, consistency with Fig. 3A would require fk_0 to be proportional to the particle size L_0 across two orders of magnitude change in L_0. Finally, the low aspect ratio GO gel[12] is much more porous ($L_c/L_0 = 1.6$) than the high aspect ratio GO gel ($L_c/L_0 = 0.3$), yet G'_0 scales with the same microstructure-dependent exponent for both gels.

In order to understand this behaviour of γ_y in the context of the crumpling model, we consider the elastic deformation of the gel up to yield point. The stored elastic energy at the yield point $0.5G\gamma_y^2$. We relate this to the energy it takes to break the contacts between neighboring crumpled nanosheets. We propose a simple relaxation dissipation model[43] to describe the yielding process. The stored elastic energy density at the yield point can be related to the energy stored in the bonds that get broken during the yielding process. In contrast to hard spheres it is difficult to characterise the bond energy between crumpled sheets in terms of bond stiffness and coordination number as

these contacts will most likely have a wide range of contact areas and therefore bond energies due to the disordered shape of crumpled sheets. Instead we introduce the area fraction $a = m(\phi - \phi_c)^x$ which denotes the fraction of the area of the free volume V_f occupied by a single sheet that is in contact with neighboring sheets with an unknown exponent x which must be positive. Since $\phi_c \ll 1$ for high aspect ratio particle suspensions,[22,32] the area fraction a should go to 1 in the theoretical limit of $\phi = 1$. Therefore the prefactor m is set to 1. The average free volume per sheet is just $V_f = L_0^2 h/\phi$ with a corresponding area $A_f = V_f^{2/3}$.

In order to model the process we equate the stored elastic energy density at the yield point to the bond energy density. If σ is the cohesive energy per area between two graphene oxide sheets in water, then the bond energy density is given by $\sigma a A_f/2V_f$. This bond density only includes bonds between neighboring sheets and not internal bonds within a crumpled sheet. The factor 2 accounts for the fact the a bond is shared by two particles. Solving for the yield strain we obtain

$$\gamma_y = \sqrt{\frac{\sigma}{c\kappa_{\alpha^{\frac{1}{3}}}}}\, h\, \phi^{\frac{1}{6}}(\phi - \phi_c)^{\frac{x}{2}-\frac{4}{3}} \qquad (2)$$

The two unknowns in this equation are the cohesion energy per area σ and the exponent x. The upper inset in Fig. 4 shows the two parameter fits for the gel with and without 0.1 M NaCl which are in good agreement with the data using $c\kappa/h^3 = 0.45$ GPa for both fits as determined earlier. Without the salt we find that $\sigma = 1.1 \pm 0.2$ mJ m^{-2} and $x = 0.66 \pm 0.05$. With salt the fit yields $\sigma = 11 \pm 2$ mJ m^{-2} and $x = 1.33 \pm 0.05$. The cohesion energies from the fit are of the same order of magnitude as in MD simulations of GO in water[18] where the free energy/area to separate two GO sheets is 5–10 mJ m^{-2}. Also, the cohesion energy is significantly higher when salt is added which is expected according to DLVO theory.[19] Fitting the yield strain of graphene in NMP (lower inset Fig. 4) we obtain $\sigma = 7 \pm 0.2$ μJ m^{-2} and $x = 0.7 \pm 0.05$. The low value of σ is consistent with the high stability of graphene in NMP suspensions.

In conclusion we find that the elasticity of particulate gels from GO and other nanosheet suspensions arise from the mechanical properties of the sheets rather than the interaction between them. Therefore these particle can be considered soft colloids. Our model based on crumpling gives the correct exponent with a prefactor that solely depends on the bending stiffness κ and thickness of the nanosheet but not on the lateral size of the particles. From the rheology we infer $\kappa = 21 \pm 14$ eV for GO which is close to simulation results.[25,33] The microstructure, which is an important parameter in modelling gel elasticity, only enters the model *via* the gelation point ϕ_c. This model should only apply to particles with nanometric thickness. It remains an open question at what bending stiffness the particles can be considered stiff such that the gel elasticity is dominated by the bond rigidity.

Author contributions

S. B. carried out the experiments and M. E. M. designed the project. Both authors analysed the data and wrote the manuscript.

Conflicts of interest

There are no conflicts to declare.

Acknowledgements

The research was supported by the grant SFI 17/CDA/4704 and SFI AMBER2 12/RC/2278. We thank T. Witten and J. Coleman for fruitful discussions.

Notes and references

1 A. Zaccone, H. Wu and E. Del Gado, *Phys. Rev. Lett.*, 2009, **103**, 208301.
2 K. A. Whitaker, Z. Varga, L. C. Hsiao, M. J. Solomon, J. W. Swan and E. M. Furst, *Nat. Commun.*, 2019, **10**, 1–8.
3 W. H. Shih, W. Y. Shih, S. I. Kim, J. Liu and I. A. Aksay, *Phys. Rev. A: At., Mol., Opt. Phys.*, 1990, **42**, 4772–4779.
4 H. Wu and M. Morbidelli, *Langmuir*, 2001, **17**, 1030–1036.
5 S. Romer, H. Bissig, P. Schurtenberger and F. Scheffold, *EPL*, 2014, **108**, 48006.
6 P. B. Laxton and J. C. Berg, *Colloids Surf., A*, 2007, **301**, 137–140.
7 L. A. Hough, M. F. Islam, P. A. Janmey and A. G. Yodh, *Phys. Rev. Lett.*, 2004, **93**, 168102.
8 S. Barwich, J. N. Coleman and M. E. Möbius, *Soft Matter*, 2015, **11**, 3159–3164.
9 A. Mourchid, E. Lecolier, H. Van Damme and P. Levitz, *Langmuir*, 1998, **14**, 4718–4723.
10 S. Naficy, R. Jalili, S. H. Aboutalebi, R. A. Gorkin III, K. Konstantinov, P. C. Innis, G. M. Spinks, P. Poulin and G. G. Wallace, *Mater. Horiz.*, 2014, **10**, 1039.
11 A. Corker, H. C.-H. Ng, R. J. Poole and E. Garca-Tuñón, *Soft Matter*, 2019, **15**, 1444–1456.
12 C. Vallés, R. J. Young, D. J. Lomax and I. A. Kinloch, *J. Mater. Sci.*, 2014, **49**, 6311–6320.
13 M. K. Blees, A. W. Barnard, P. A. Rose, S. P. Roberts, K. L. McGill, P. Y. Huang, A. R. Ruyack, J. W. Kevek, B. Kobrin and D. A. Muller, *et al.*, *Nature*, 2015, **524**, 204–207.
14 M. Fokker, S. Janbaz and A. Zadpoor, *RSC Adv.*, 2019, **9**, 5174–5188.
15 R. D. Piner, T. T. Xu, F. T. Fisher, Y. Qiao and R. S. Ruoff, *Langmuir*, 2003, **19**, 7995–8001.
16 S. Gambhir, R. Jalili, D. L. Officer and G. G. Wallace, *NPG Asia Mater.*, 2015, **7**, e186.
17 K. P. Loh, Q. Bao, G. Eda and M. Chhowalla, *Nat. Chem.*, 2010, **2**, 1015–1024.
18 C.-J. Shih, S. Lin, R. Sharma, M. S. Strano and D. Blankschtein, *Langmuir*, 2012, **28**, 235–241.

19 L. Wu, L. Liu, B. Gao, R. Muñoz-Carpena, M. Zhang, H. Chen, Z. Zhou and H. Wang, *Langmuir*, 2013, **29**, 15174–15181.
20 F. Del Giudice and A. Q. Shen, *Curr. Opin. Chem. Eng.*, 2017, **16**, 23–30.
21 F. D. Giudice, B. V. Cunning, R. S. Ruoff and A. Q. Shen, *Rheol. Acta*, 2018, **57**, 293–306.
22 E. Han, J. Yu, E. Annevelink, J. Son, D. A. Kang, K. Watanabe, T. Taniguchi, E. Ertekin, P. Y. Huang and A. M. van der Zande, *Nat. Mater.*, 2020, **19**, 305–309.
23 P. Poulin, R. Jalili, W. Neri, F. Nallet, T. Divoux, A. Colin, S. H. Aboutalebi, G. Wallace and C. Zakri, *Proc. Natl. Acad. Sci. U. S. A.*, 2016, **113**, 11088–11093.
24 L. Liu, X. Li, Z. Liu, S. Dai, X. Huang and J. Zhao, *Nanoscale*, 2020, **12**, 1623–1628.
25 A. Incze, A. Pasturel and P. Peyla, *Phys. Rev. B: Condens. Matter Mater. Phys.*, 2004, **70**, 212103.
26 (*a*) A. P. Philipse, *Langmuir*, 1996, **12**, 1127–1133; (*b*) A. P. Philipse, *Langmuir*, 1996, **12**, 5971.
27 H. King Jr, S. T. Milner, M. Y. Lin, J. P. Singh and T. Mason, *Phys. Rev. E: Stat., Nonlinear, Soft Matter Phys.*, 2007, **75**, 021403.
28 M. van Hecke, *J. Phys.: Condens. Matter*, 2010, **22**, 033101.
29 V. Trappe and P. Sandkühler, *Curr. Opin. Colloid Interface Sci.*, 2004, **8**, 494–500.
30 H. Tanaka, J. Meunier and D. Bonn, *Phys. Rev. E: Stat., Nonlinear, Soft Matter Phys.*, 2004, **69**, 031404.
31 M. J. Solomon and P. T. Spicer, *Soft Matter*, 2010, **6**, 1391–1400.
32 P.-K. Kao, M. J. Solomon and M. Ganesan, *Soft Matter*, 2022, **18**, 1350–1363.
33 S. Lin, C.-J. Shih, V. Sresht, A. G. Rajan, M. S. Strano and D. Blankschtein, *Adv. Colloid Interface Sci.*, 2017, **244**, 36–53.
34 J. L. Suter and P. V. Coveney, *Sci. Rep.*, 2021, **11**, 1–11.
35 K. Matan, R. B. Williams, T. A. Witten and S. R. Nagel, *Phys. Rev. Lett.*, 2002, **88**, 076101.
36 T. A. Witten, *Rev. Mod. Phys.*, 2007, **79**, 643.
37 G. Wang, Z. Dai, J. Xiao, S. Z. Feng, C. Weng, L. Liu, Z. Xu, R. Huang and Z. Zhang, *Phys. Rev. Lett.*, 2019, **123**, 116101.
38 Y.-T. Fu, G. D. Zartman, M. Yoonessi, L. F. Drummy and H. Heinz, *J. Phys. Chem. C*, 2011, **115**, 22292–22300.
39 R. De Rooij, D. Van den Ende, M. H. Duits and J. Mellema, *Phys. Rev. E: Stat. Phys., Plasmas, Fluids, Relat. Interdiscip. Top.*, 1994, **49**, 3038.
40 D. A. Kunz, E. Max, R. Weinkamer, T. Lunkenbein, J. Breu and A. Fery, *Small*, 2009, **5**, 1816–1820.
41 L. Liu, J. Zhang, J. Zhao and F. Liu, *Nanoscale*, 2012, **4**, 5910–5916.
42 A. G. Kelly, D. O'Suilleabhain, C. Gabett and J. N. Coleman, *Nat. Rev. Mater.*, 2022, **7**, 217–234.
43 T. A. Witten and P. A. Pincus, *Structured fluids*, Oxford University Press, 2004.

